

June 22, 2022

**Luminescence dating report for Dr. Michael Polenz & Dr. Alex Steely, from the Washington Geological Survey**

ISGS code	Sample	Grain Size ( $\mu\text{m}$ )	Equivalent dose (Gy) <sup>1</sup>	Dose rate (Gy/ka)	Age (ka) <sup>1</sup>	n (accepted/total)
798	MLm047b	180 - 250	381 $\pm$ 58	2.04 $\pm$ 0.06	187.0 $\pm$ 29.3	10/17
799	MLm065c	150 - 250	285 $\pm$ 37	2.00 $\pm$ 0.07	142.6 $\pm$ 19.1	11/13
800	AS05SEP21-1	125 - 150	96 $\pm$ 10	2.26 $\pm$ 0.08	42.3 $\pm$ 4.7	11/93
801	AS05SEP21-2	150 - 250	109 $\pm$ 11	2.23 $\pm$ 0.08	49.1 $\pm$ 5.4	12/23
802	AS05SEP21-4	150 - 250	89 $\pm$ 7	2.23 $\pm$ 0.08	40.0 $\pm$ 3.4	10/21
803	AS05SEP21-5	150 - 250	67 $\pm$ 4	3.12 $\pm$ 0.10	21.5 $\pm$ 1.6	12/12

<sup>1</sup> Huntley and Lamothe (2001) fading corrected values

Infrared stimulated luminescence (IRSL) dating was measured on K-feldspar, on small aliquots. The age was corrected for anomalous fading. Uncertainties are reported at a  $1\sigma$  significance, providing a level of confidence of approximately 67%. The uncertainties combine random and systematic errors, added in quadrature. Further details can be found in the report.

**Sebastien Huot, Ph.D.**

Illinois State Geological Survey

Champaign, Illinois

shuot@illinois.edu

+1-217-300-2579 (office)

This is a report on the infrared stimulated luminescence (IRSL) dating of six samples delivered to us by Dr. Michael Polenz & Dr. Alex Steely, in Autumn 2021. The samples were retrieved in opaque tubes, from natural outcrops. The depositional environment is interpreted as glaciofluvial. Both MLmxxx samples are expected to be very old (less than 1 million year). Partial bleaching might play a significant role, for the AS05SEP21-x samples, especially if these turns out to be young. For the purposes of internal identification, we labeled these samples ISGS 798 - 803.

## 1. Sample preparation and equipment

The tubes were opened, and a mineral extraction was conducted in a subdued orange light environment. One inch of sediment (i.e. the external portion) was removed from both ends of each tube because these might have been partially exposed to light during sampling. Sediment from the external portions was used to measure the *in situ* water content and its radioactive content (uranium, thorium, and potassium), both for dose rate calculation. K-feldspar and quartz minerals for IRSL/OSL dating were extracted from the remainder (inner portion) of each tube.

These minerals were wet sieved to retrieve the 125- to 250- $\mu\text{m}$  grain size. A hydrochloric acid attack (HCl, 10%) was applied to dissolve any carbonate minerals that might be present. Using a heavy liquid solution (2.58 g/mL) of lithium heteropolytungstate (LST), we separated K-feldspar (<2.58) from the quartz and Na-feldspar minerals (>2.58). The K-feldspar were further sized at 125- to 150-  $\mu\text{m}$  grain size. For quartz minerals, further purification was done with a hydrofluoric acid (HF) attack (40% for 1 hour) to dissolve any remaining impurities. A second HCl attack was performed to dissolve calcium fluorite minerals, a potential by-product of HF dissolution of Ca-rich silicates. Finally, the purified quartz extracts were again sieved, at 150  $\mu\text{m}$ , to remove partially dissolved impurities. A purity check was performed by doing an infrared over blue OSL stimulation. These quartz samples showed no significant contamination from feldspar.

The initial luminescence signal observed from these K-feldspar minerals were unusually dim. To further increase the purity of these K-feldspar, we made use of a Frantz magnetic separator and relied on the non-magnetic fraction (0.7 ampere) for IRSL dating. A lot of minerals had a paramagnetic property. Personal experience as shown me that these paramagnetic minerals, contaminating the K-feldspar low density fraction do not emit any luminescence signal. These purified K-feldspar grains displayed a brighter luminescence signal. Not as bright as would be expected, from < ordinary > K-feldspar minerals. The relative amount of K-feldspar minerals, purified from these samples, is still larger than the abundance of potassium measured in these sediments (c.f. dose rate section). Mostly likely, a contamination remains. Fortunately, the luminescence measurements are carried out with infrared LED. Stimulation by infrared is an unusual luminescence characteristic, almost exclusively found in feldspar and plagioclase minerals (Krbetschek et al., 1997).

For sample MLm047b (ISGS 798), we also extracted Na-feldspar. The density was bracketed between 2.58 - 2.65 g/mL. We also made judicious use of a Frantz magnetic separator (0.7 ampere).

To obtain the dose rate, sediments from the external portion of each sampling tube were dried, and a representative portion was encapsulated in thin disk-shaped containers (~20 g) and sealed with 2 layers of epoxy gel. A minimum waiting time of 21 days after sealing is recommended to restore the radioactive equilibrium of radon-222 daughter products (Gilmore, 2008). The specific activities (Bq/kg) were measured with a broad-energy high-purity germanium detector (BEGe), in a planar configuration, shielded by 15 cm of lead. Efficiency calibration of the detector was obtained with a set of six certified standards (IAEA-RGU-1, IAEA-RGTh-1, IAEA-RGK-1, IAEA-385, NIST 4350b, and NIST 4355).

## 2. Equivalent dose (De) measurements

For the equivalent dose (De) measurements, we relied on an automated Lexsyg Smart system equipped with a set of green (525-nm) and infrared (850-nm) LEDs for light stimulation. Detection was done in UV-blue light (combination of Schott BG3 glass and Delta BP 365/50 EX interference filters) for quartz. For K-feldspar minerals, the detection was done in blue light (combination of Schott BG39 glass and Semrock 414/46 Brightline HC interference filters). For Na-feldspar minerals, the detection was done in orange light (combination of Schott BG39 glass and Semrock 571/72 Brightline HC interference filters). For both K-feldspar and Na-feldspar, grains were dispensed on a small area, 1 mm in diameter; around 10 - 20 grains were dispensed on each cup. The Lexsyg Smart was used for samples MLm047b and MLm065c.

For the other samples, AS05SEP21-1, AS05SEP21-2, AS05SEP21-4, and AS05SEP21-5, their luminescence measurements were acquired with an automated Risø TL-DA-20 system, equipped with a set of blue (470 nm) and infrared (870 nm) LEDs, for light stimulation. Detection was made in the UV (Hoya U340 filter) for quartz or in the blue (combination of Schott BG39 and Corning 7-59 glass filters) for K-feldspar. For each sample, we dispensed quartz grains over a small area (2 mm), onto a silicon oil covered stainless disk (10 mm diameter). Around 50 grains were dispensed on each disk. For K-feldspar, grains were dispensed on a small area, 1 mm in diameter; around 10 - 20 grains were dispensed on the disk's center.

IRSL measurements were carried out with a single-aliquot regenerative dose (SAR) protocol (Table 1a, 1b). The optimal measurement parameters were selected by a dose recovery test (latent dose bleached with sunlight for 1 day). An initial dose was given at first (that was a close match to the measured equivalent dose for each sample: 34 or 345 Gy, for samples 800-803 or 798-799, respectively) and it was subsequently recovered by measuring its equivalent dose with the SAR protocol. The samples responded reasonably well to the treatment. From this we selected a preheat temperature (Lx and Tx) of 250°C or 220°C (held for 60 seconds; Huot and Lamothe, 2003), for samples 800-803 or 798-799, respectively. The dose recovery test was performed for every sample using the most appropriate temperature. It yielded an average measured-to-given dose ratio of  $1.09 \pm 0.01$  ( $n = 3$ ) or  $1.00 \pm 0.02$  ( $n = 3$ ), for samples 800-803 or 798-799, respectively. This outcome is positive. Considering this result, we opted to select the parameters in Table 1a, 1b.

Table 1a. Measurement steps for the single-aliquot regenerative protocol (Huot and Lamothe, 2003; Murray and Wintle, 2000). For samples 798 and 799.

Step	Procedure (K-feldspar)
1	Regeneration <sup>1</sup> /natural dose
2	Preheat (220 °C), hold for 60 seconds
3	Pause <sup>2</sup>
4	IRSL stimulation with IR LEDs at 50 °C for 100 seconds ( $L_x$ )
5	Test dose beta irradiation (173 Gy)
6	Preheat (220 °C) for 60 seconds
7	IRSL stimulation with IR LEDs at 50 °C for 100 seconds ( $T_x$ )
8	Repeat Steps 1–7 with further regeneration doses

<sup>1</sup> For equivalent dose measurements, we gave a range of laboratory-induced doses that would properly encompass the variability of the observed natural luminescence.

<sup>2</sup> There was no pause for equivalent dose measurements. A pause was observed here for anomalous fading measurements.

Table 1b. Measurement steps for the single-aliquot regenerative protocol (Huot and Lamothe, 2003; Murray and Wintle, 2000). For samples 800 to 803.

Step	Procedure (K-feldspar)
1	Regeneration <sup>1</sup> /natural dose
2	Preheat (250 °C), hold for 60 seconds
3	Pause <sup>2</sup>
4	IRSL stimulation with IR LEDs at 50 °C for 100 seconds ( $L_x$ )
5	Test dose beta irradiation (20 Gy)
6	Preheat (250 °C) for 60 seconds
7	IRSL stimulation with IR LEDs at 50 °C for 100 seconds ( $T_x$ )
8	Repeat Steps 1–7 with further regeneration doses

<sup>1</sup> For equivalent dose measurements, we gave a range of laboratory-induced doses that would properly encompass the variability of the observed natural luminescence.

<sup>2</sup> There was no pause for equivalent dose measurements. A pause was observed here for anomalous fading measurements.

## 2.1 Equivalent dose calculation

For the equivalent dose, all calculations were made using the “late light” approach for background subtractions, by taking the initial 5 data channels (5 seconds) from the IRSL decay curve and removing the background from the end of the stimulation curve (30 data channels, 30 seconds; Figure 1a, 1b).

## Lexsyg Smart luminescence system

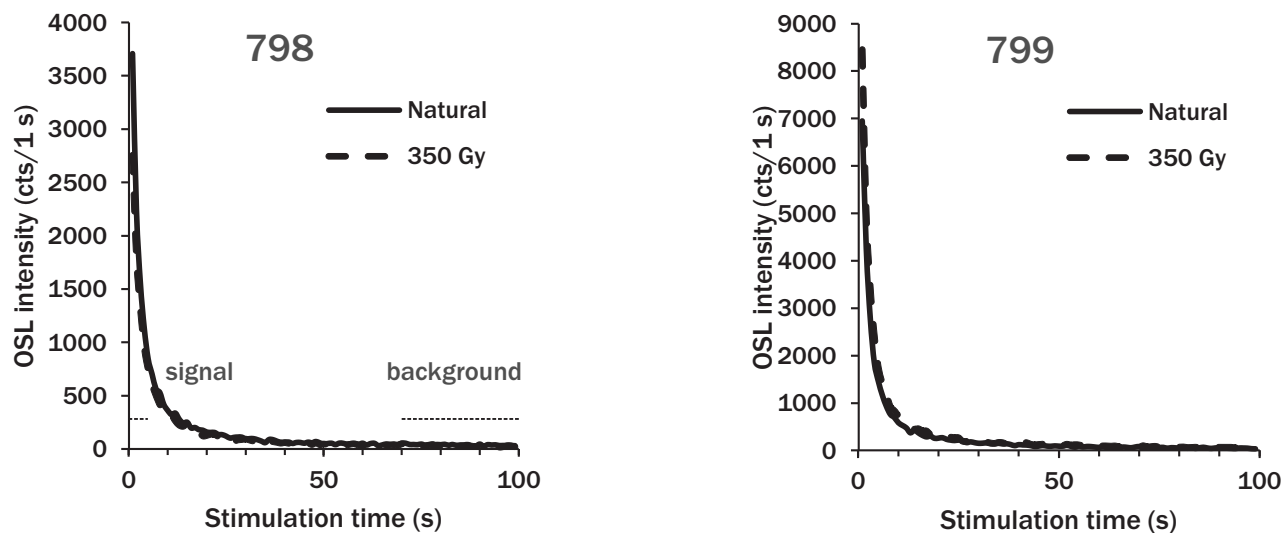


Figure 1a. Typically IRSL decay curve, for a naturally dose aliquot (solid curve) or laboratory-induced dose (dashed curve, in Gy). The area under the curve is proportional to the dose of radiation stored within the mineral. Their luminescence growth curve and fading rate are shown in Figure 2 and 3.

## Risoe luminescence system

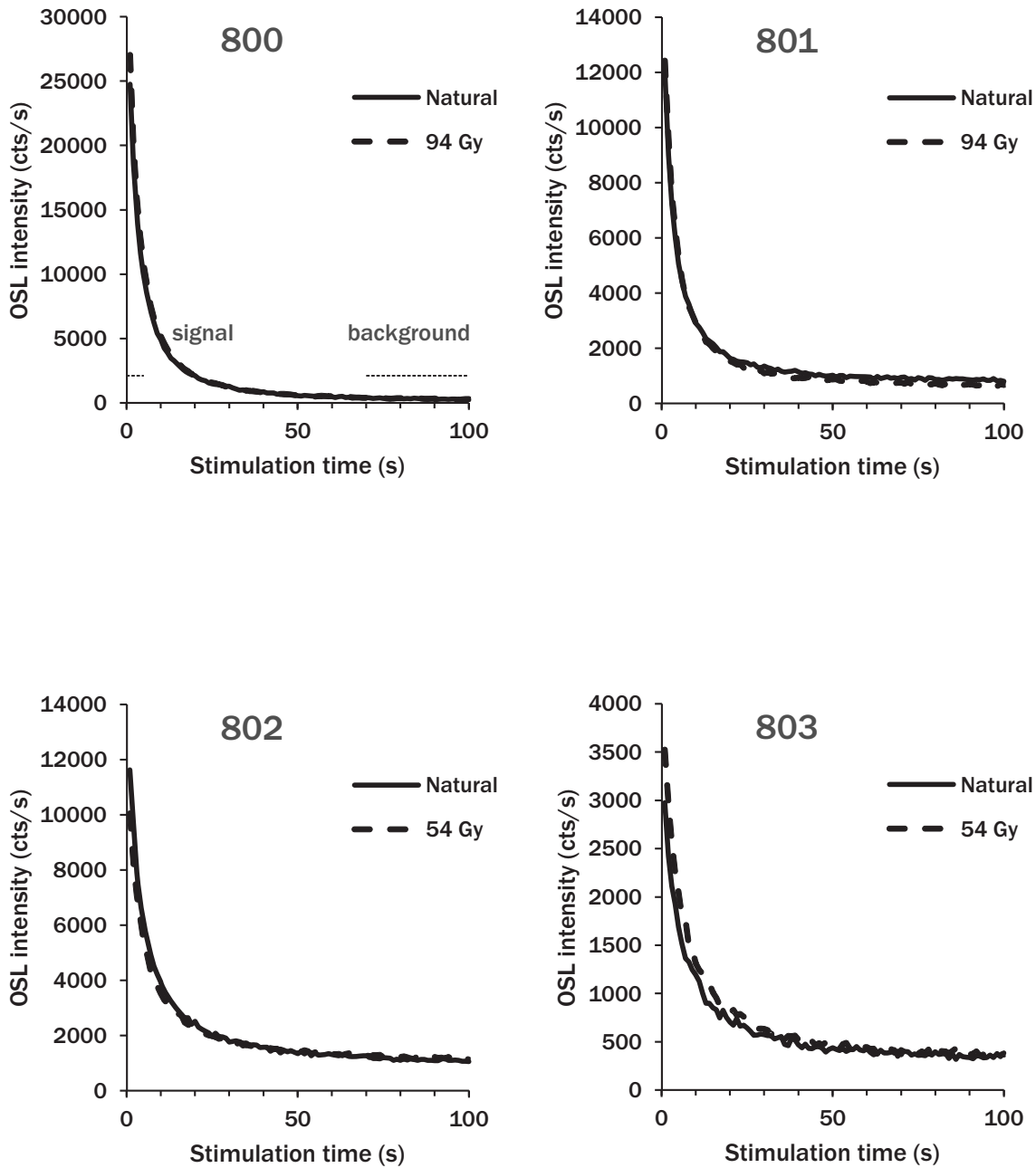


Figure 1b. Typically IRSL decay curve, for a naturally dose aliquot (solid curve) or laboratory-induced dose (dashed curve, in Gy). The area under the curve is proportional to the dose of radiation stored within the mineral. Their luminescence growth curve and fading rate are shown in Figure 2 and 3.

Uncertainties relied on Poisson statistics. For curve fitting, we also propagated the uncertainties from the optimized luminescence growth curve parameters. In addition, when the observed scatter about the best fit regression line was too high, the uncertainties were increased (Figure 2a, 2b). For this, we relied on the one-tailed probability  $\chi^2$  distribution, with  $N - 3$  degrees of freedom (where  $N$  is the number of measured data points). When the probability was lower than 15% (i.e., the data points scattered above and beyond the best fit line), the uncertainties for the optimized parameters were expanded by Student's  $t$  values for  $N - 3$  degrees of freedom (Brooks et al., 1972; Ludwig, 2003).

## 2.2. Anomalous fading

The luminescence of feldspar is known to underestimate the 'true' burial age, typically by about 30 to 50 % (Aitken, 1998). The cause is known to us: anomalous fading (Wintle, 1973). Luminescence dating is akin to a filling a glass with water. At time zero, the glass is empty (i.e. the zeroing effect of sunlight). You pour water into it, at a constant rate (dose rate), but stop before reaching the top (sampling). The volume of water contained in the glass represents the equivalent dose in luminescence (the total amount of radiation energy trapped by the mineral during burial). By dividing the volume (equivalent dose) by the rating of water filling (dose rate), we can calculate when was the glass empty (length of burial).

Now, what if there is a very small hole in the glass. As you pour water into it, you lose water through that hole, at a steady rate. Now, the volume of water that remains in the glass underestimate the real amount of water that was poured in it. If you can measure the size of the hole, it is possible to calculate what would have been the real amount of water contained in the glass.

The luminescence of quartz (our workhorse in luminescence dating) is akin to a perfect glass, whereas K-feldspar is that of a glass with a hole. At the time this phenomenon was first describe in feldspar, the mechanism underlying that lost, or fading, was unknown to us; hence, it was termed 'anomalous fading'. It was 'anomalous' because from thermodynamic principles, it is expected that a trapped electron would remain so for many millions of years (i.e. water can evaporate from your glass) at room temperature (i.e. just like water, where the evaporation rate is temperature dependent, so is the thermal lifetime of a trapped electron). Yet, trapped elections in feldspar are leaking faster than they should and that rate of leakage is independent of temperature. Hence, anomalous!

Nowadays, we know how to deal with it. We know how to measure the size of the hole (fading rate; Auclair et al., 2003) and we know how to properly correct for it (e.g. Huntley and Lamothe, 2001).

Anomalous fading measurements were performed on the same aliquot previously used for equivalent dose measurements. After the equivalent dose measurement cycles, the aliquots were taken outside the luminescence system, for sunlight bleaching (2 days), before passing over the anomalous fading sequence of measurements. It also employed the SAR protocol (table 1a, 1b), with two adjustments. The laboratory-induced dose (step 1) was fixed, at 174 Gy, along with a test

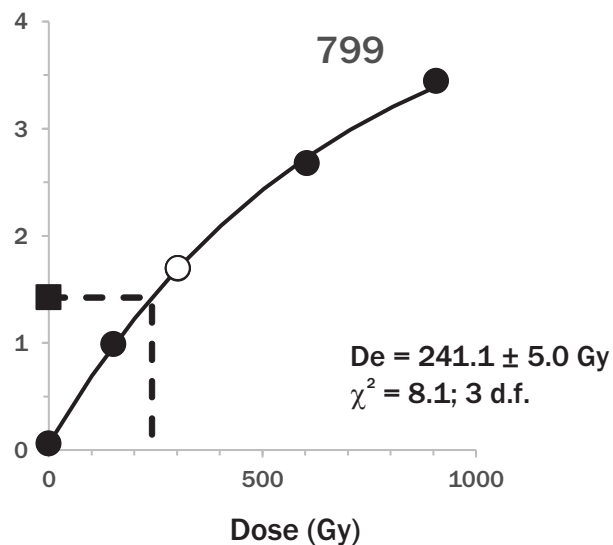
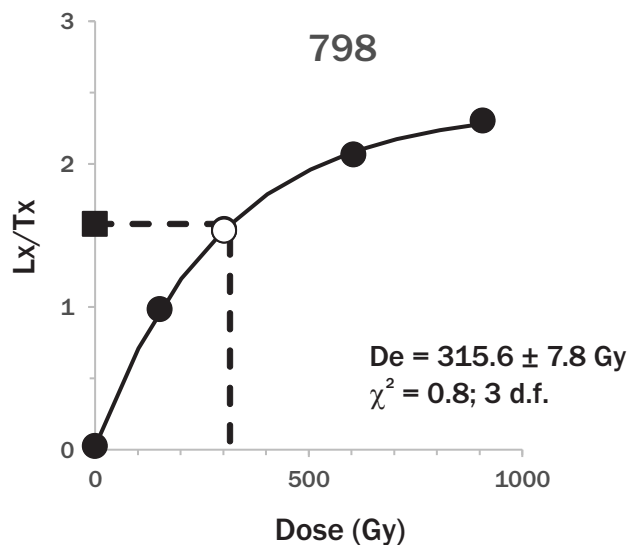


Figure 2a. Luminescence dose response curve for the same aliquots shown in Figure 1. Each point corresponds to the IRSL ( $L_x$ ; measurement step 4) of a natural (square) or laboratory-induced dose (filled circles)), normalized by the luminescence response to a fixed test dose ( $T_x$ ; measurement step 7). A repeat measurement (the recycling test; open circles) was performed at the end. The equivalent dose is obtained by interpolation. For the aliquots shown here, the observed measurements scatter well around the predicted best-fit curve.



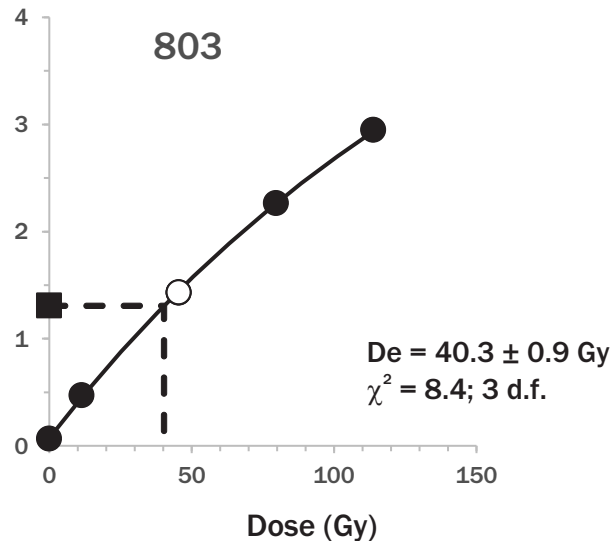
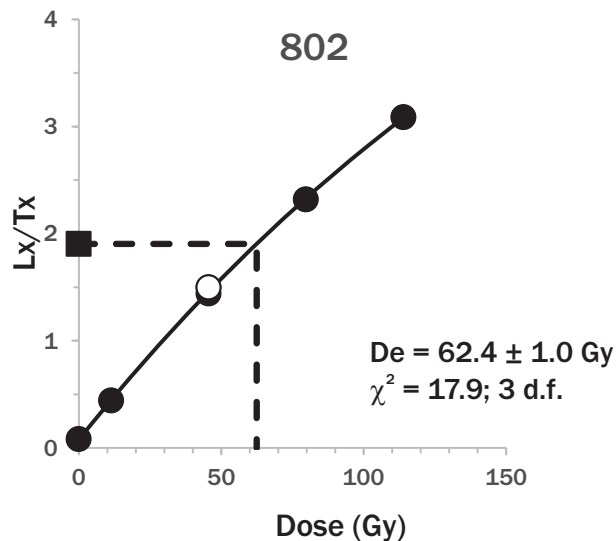
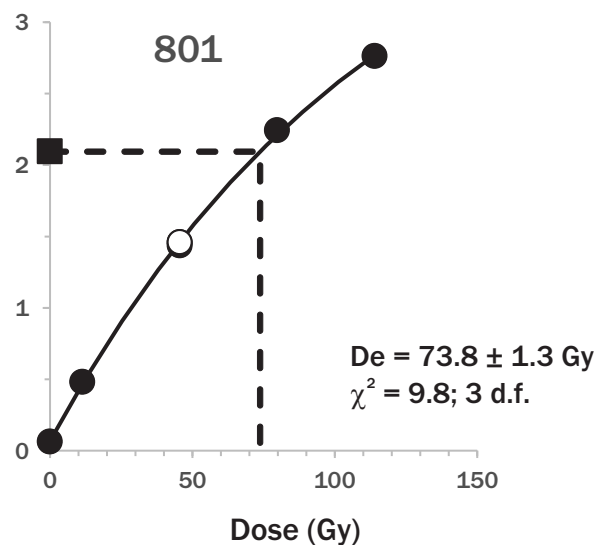
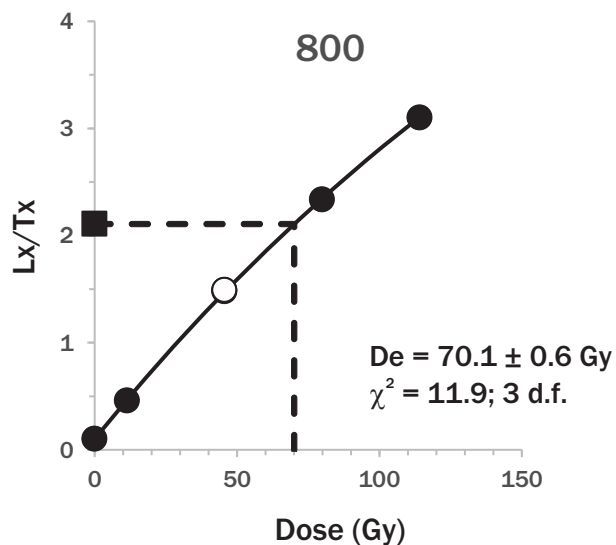


Figure 2b. Luminescence dose response curve for the same aliquots shown in Figure 1. Each point corresponds to the IRSL ( $L_x$ ; measurement step 4) of a natural (square) or laboratory-induced dose (filled circles)), normalized by the luminescence response to a fixed test dose ( $T_x$ ; measurement step 7). A repeat measurement (the recycling test; open circles) was performed at the end. The equivalent dose is obtained by interpolation. For the aliquots shown here, the observed measurements scatter well around the predicted best-fit curve.

dose (step 5) of 87 Gy. Also, there was a ‘pause’ in effect, at step 3, which ranged from 10 minutes up to 30 hours (Figure 3a, 3b; Auclair et al., 2003).

## 2.3 Age distribution

A weighted average (using the central age model; Galbraith et al., 1999) was used in all calculations, except when noted otherwise. The central age model provides an overdispersion parameter. This parameter characterizes the degree to which the observed weighted distribution is consistent with the predicted weighted distribution from the observed data. At 0%, the observed distribution is equal to the statistical prediction. In luminescence dating, it is common for the observed distribution to be slightly larger than the expected distribution by a value of approximately 20%. This means that the calculated uncertainties tend to underestimate the “real” uncertainties because of intrinsic (e.g., instrumental uncertainties, luminescence characteristics of quartz and K-feldspar) or extrinsic (e.g., partial bleaching, external beta microdosimetry) factors. The central age model expands the age uncertainty in an attempt to account for this discrepancy. Here, the overdispersions are near the average (Table 2; Figure 4). For samples MLm047b and MLm065c, the overdispersion is slightly larger; the betrays the difficulty is measuring older ages!

Table 2. Age overdispersion parameters<sup>1</sup>

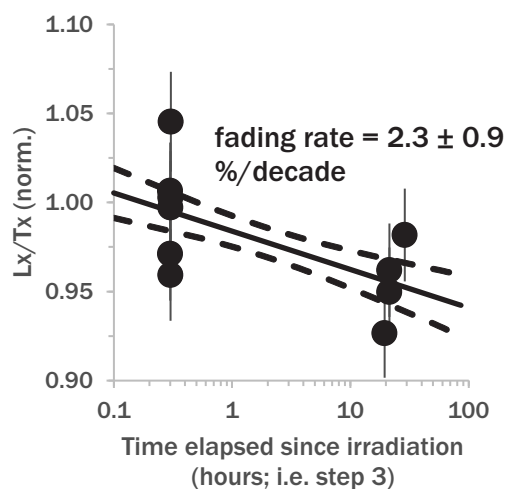
ISGS code	Sample	Overdispersion (%)
798	MLm047b	41 ± 12
799	MLm065c	35 ± 10
800	AS05SEP21-1	24 ± 8
801	AS05SEP21-2	27 ± 8
802	AS05SEP21-4	21 ± 6
803	AS05SEP21-5	18 ± 6

<sup>1</sup>A value of 20% is typical in luminescence

## 2.4 Fading corrected age

Measured IRSL ages were corrected for anomalous fading using the Huntley and Lamothe (2001). The fading rate was measured for each equivalent dose, aliquot by aliquot. After the equivalent dose measurement, the aliquots were bleached under normal sunlight, for one day. After, the anomalous fading measurement was initiated (Table 1a, 1b). Thus, pairing equivalent dose with anomalous fading rate, aliquot by aliquot.

798



799

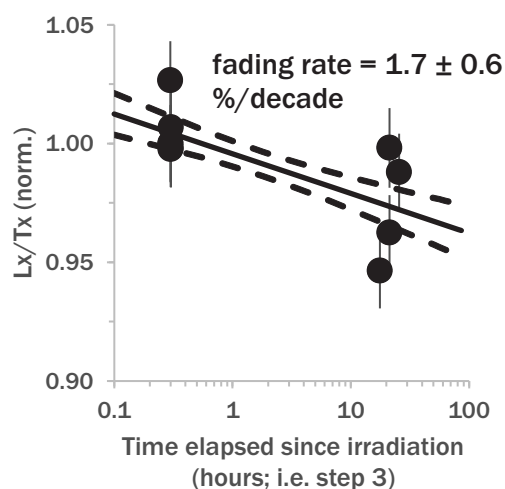
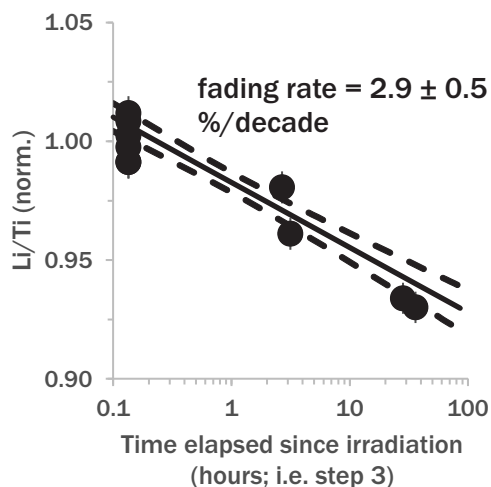
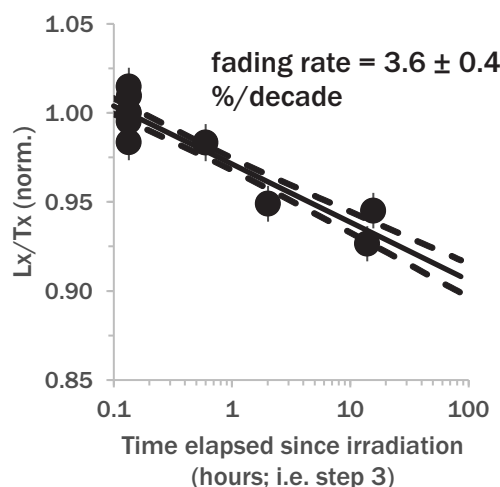


Figure 3a. Anomalous fading measurement, for a representative aliquot of each sample (the same shown in Figure 1 and 2). Repeated measurement cycles (Table 1) are made, on the same aliquot, with different delays between the irradiation and the IRSL measurement (i.e. step 3). The slope is proportional to the fading rate, used in the fading correction model. The 2 dashed lines represent the  $1\sigma$  error envelopes. Note the logarithmic time axis.

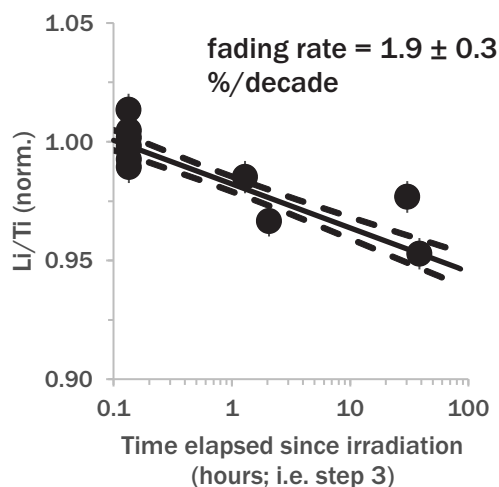
800



801



802



803

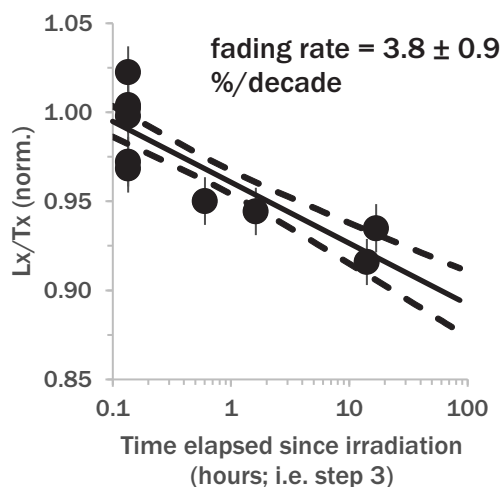
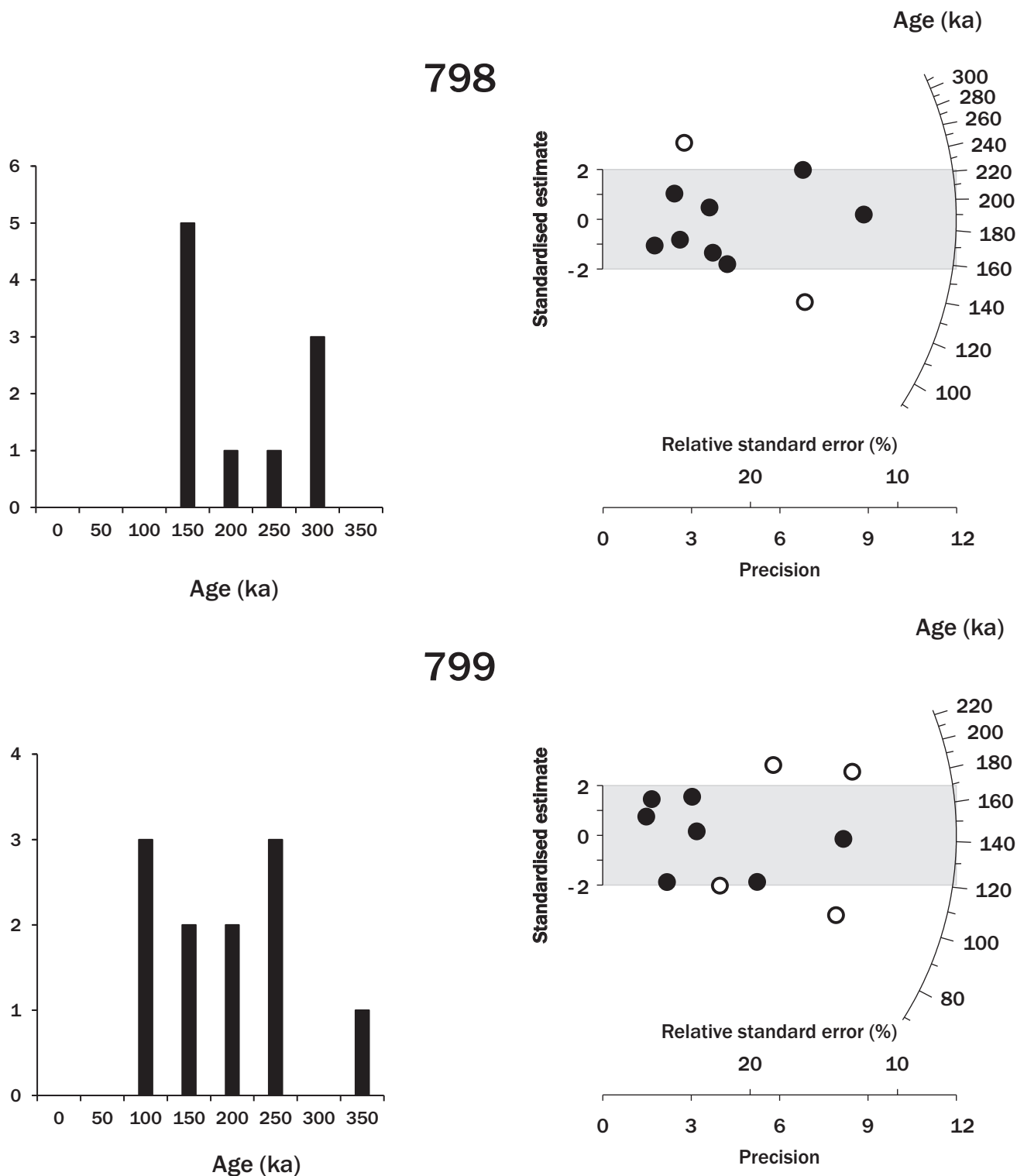
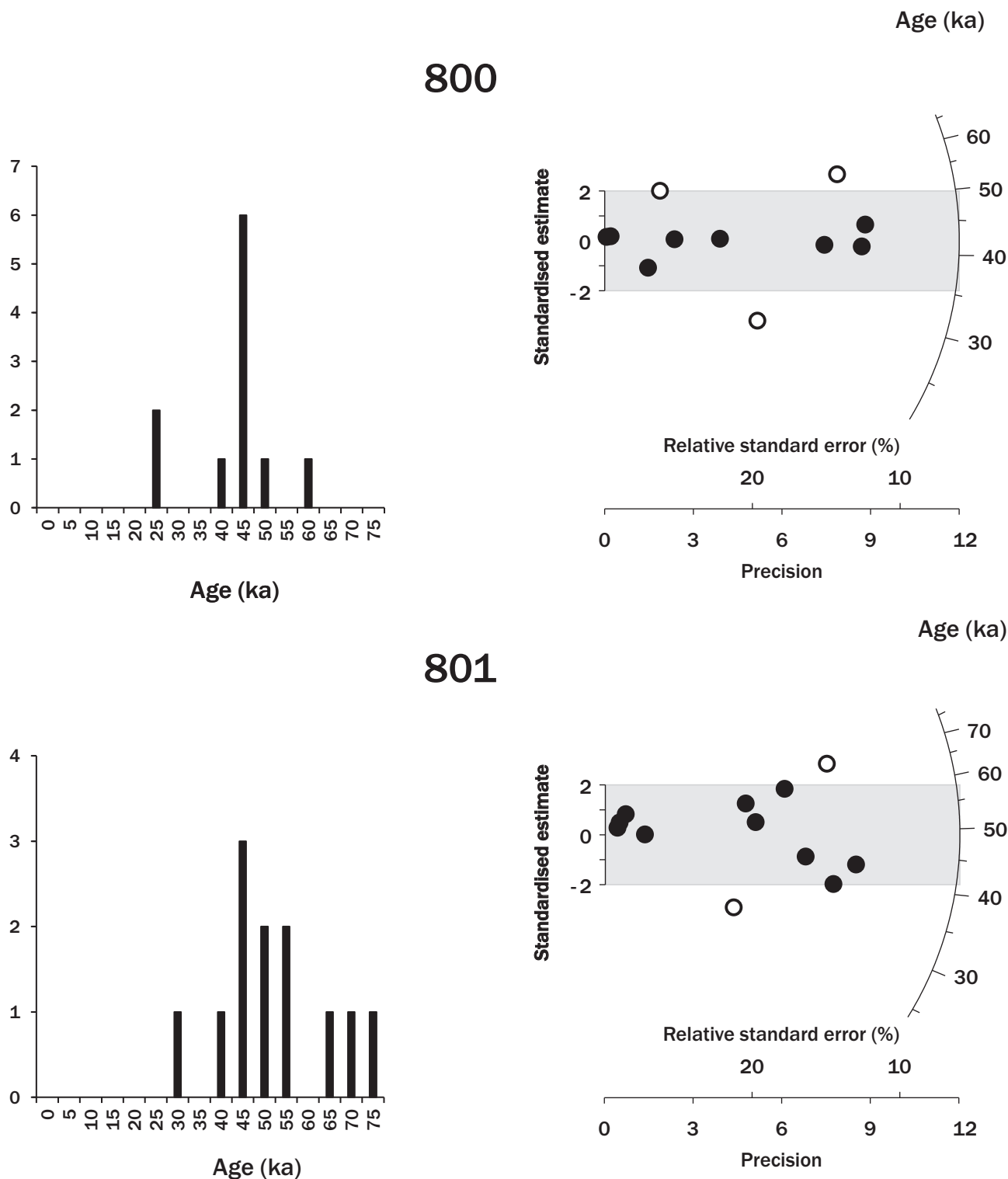


Figure 3b. Anomalous fading measurement, for a representative aliquot of each sample (the same shown in Figure 1 and 2). Repeated measurement cycles (Table 1) are made, on the same aliquot, with different delays between the irradiation and the IRSL measurement (i.e. step 3). The slope is proportional to the fading rate, used in the fading correction model. The 2 dashed lines represent the  $1\sigma$  error envelopes. Note the logarithmic time axis.



**Figure 4.** Age distributions, as a histogram and a radial plot, for all samples. Each circle on the radial plot represents the age and uncertainty, for a single aliquot. The age is read on the arc axis, by drawing a straight line from (0, 0), passing through a circle and intersecting the radial axis (log scale). The (0, 0) coordinate corresponds to a 0 standardised estimate (y-axis) and 0 precision (x-axis). The uncertainty is read on the horizontal axis, by drawing a perpendicular line reaching a circle. Hence, two aliquots, having the same age, but with different uncertainty, will lay on the same straight line (from (0, 0) to the radial axis). The aliquot with the smaller uncertainty (higher precision) will be closer to the arc. Values (filled circles) within the light grey shaded band are consistent (at  $2\sigma$ ) with the weighted mean (Central Age Model). A cluster of aliquots within this shaded band expresses confidence that we have a population of grains consistent with a single age.



**Figure 4.** Age distributions, as a histogram and a radial plot, for all samples. Each circle on the radial plot represents the age and uncertainty, for a single aliquot. The age is read on the arc axis, by drawing a straight line from (0, 0), passing through a circle and intersecting the radial axis (log scale). The (0, 0) coordinate corresponds to a 0 standardised estimate (y-axis) and 0 precision (x-axis). The uncertainty is read on the horizontal axis, by drawing a perpendicular line reaching a circle. Hence, two aliquots, having the same age, but with different uncertainty, will lay on the same straight line (from (0, 0) to the radial axis). The aliquot with the smaller uncertainty (higher precision) will be closer to the arc. Values (filled circles) within the light grey shaded band are consistent (at  $2\sigma$ ) with the weighted mean (Central Age Model). A cluster of aliquots within this shaded band expresses confidence that we have a population of grains consistent with a single age.

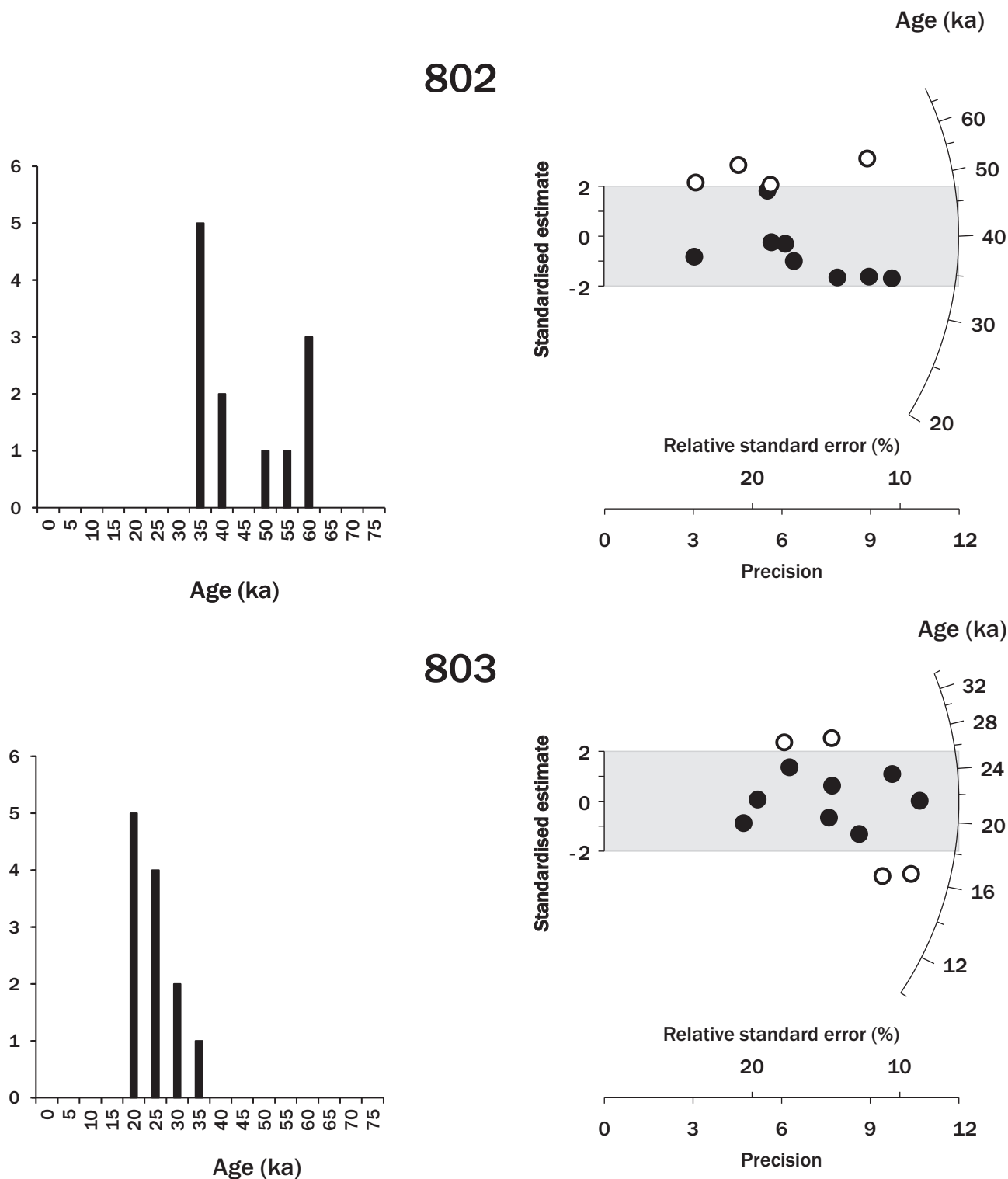


**Figure 4.** Age distributions, as a histogram and a radial plot, for all samples. Each circle on the radial plot represents the age and uncertainty, for a single aliquot. The age is read on the arc axis, by drawing a straight line from (0, 0), passing through a circle and intersecting the radial axis (log scale). The (0, 0) coordinate corresponds to a 0 standardised estimate (y-axis) and 0 precision (x-axis). The uncertainty is read on the horizontal axis, by drawing a perpendicular line reaching a circle. Hence, two aliquots, having the same age, but with different uncertainty, will lay on the same straight line (from (0, 0) to the radial axis). The aliquot with the smaller uncertainty (higher precision) will be closer to the arc. Values (filled circles) within the light grey shaded band are consistent (at  $2\sigma$ ) with the weighted mean (Central Age Model). A cluster of aliquots within this shaded band expresses confidence that we have a population of grains consistent with a single age.

The < as measured > equivalent dose from aliquot was corrected with the aid of the Huntley and Lamothe (2001) model. The Huntley and Lamothe (2001) has a limitation: it is accurate, as long as the equivalent dose is within the linear approximation of the luminescence growth curve. For the AS05SEP21-x samples, the luminescence growth curve can be approximated to a simple straight line for radiation doses easily up to 100 Gy (Figure 2). This is more than the < as measured > (i.e. before fading correction) equivalent doses for these samples (Table 3). For the older samples, the linear approximation still looks reasonable, for sample MLm065c. A bit less, for sample MLm047b, but approximation should still yield a reasonable age (Buylaert et al., 2008). Over the years, this model has proven to be highly successful in yielding accurate ages, whenever an independent assessment could be made.

Table 3. Comparison of as measured versus fading corrected age (ka), along with fading rate

ISGS code	sample	as measured age	Huntley and Lamothe (2001)	average fading rate (%/decade)
798	MLm047b	157 ± 37	187 ± 29	4.4 ± 1.9
799	MLm065c	86 ± 15	143 ± 19	2.4 ± 0.6
800	AS05SEP21-1	28 ± 4	42 ± 5	3.5 ± 0.3
801	AS05SEP21-2	30 ± 3	49 ± 5	6.4 ± 0.7
802	AS05SEP21-4	33 ± 3	40 ± 3	3.1 ± 0.3
803	AS05SEP21-5	15 ± 1	21 ± 2	4.5 ± 0.3

## 2.5 Quartz and Na-feldspar minerals

An attempt was made to measure the equivalent dose with quartz minerals. A clear advantage of quartz over K-feldspar is resetting of the latent luminescence, while exposed to sunlight (i.e. partial bleaching, during the last sedimentary cycle). It requires considerably less exposure time to properly reset quartz minerals (Godfrey-Smith et al., 1988). Unfortunately, the luminescence signal of quartz minerals was showing undesirable luminescence characteristics.

We also had a look at Na-feldspar. This mineral has the advantage of measuring older ages, potentially up to 1 million years. Whereas K-feldspar and quartz minerals have a traditional maximum limit of 500 ka and 100 ka. We also did a few measurements with Na-feldspar, because the initial results (table 4b) were corroborating those obtained with K-feldspar.

Nevertheless, we provide the few luminescence age results obtained here, if only to show that they are in the right ballpark range of the IRSL ages (Table 4a, 4b).



Table 4a. Age estimate from quartz OSL (150 – 250  $\mu\text{m}$ )

ISGS code	sample	Quartz age (ka)	K-feldspar (ka)
800	AS05SEP21-1	$33 \pm 12$	$42 \pm 5$

Table 4b. Age estimate from Na-feldspar (150 – 250  $\mu\text{m}$ ), before fading correction

ISGS code	sample	Na-feldspar age (ka)	K-feldspar (ka)
798	MLm047b	$159 \pm 14$	$157 \pm 37$

### 3. Dose rate

The water content was measured for each sample. The as-received water content was very humid (Table 5). It seems reasonable, to expect this state would have held, for most of the sediments' burial history. Given this, we opted for the values presented in the table. We assigned a water content uncertainty of 5 % to account for possible variation during the entire length of burial. The bulk density was measured for these samples; it averaged at 1.6 g/cm<sup>3</sup>.

Table 5. Water content, measured from the sample, with the value presumed to have prevailed during the burial, along with density

ISGS code	Sample	in situ (%)	presumed (%)	density (g/cm <sup>3</sup> )
798	MLm047b	25	$25 \pm 5$	1.5
799	MLm065c	29	$30 \pm 5$	1.3
800	AS05SEP21-1	12	$12 \pm 5$	1.8
801	AS05SEP21-2	10	$10 \pm 5$	1.6
802	AS05SEP21-4	9	$10 \pm 5$	1.7
803	AS05SEP21-5	26	$25 \pm 5$	1.4

Waiting times of around 30 days were observed before measuring the radioactive activities of uranium, thorium, and potassium, from which we can derive contributions from alpha, beta, and gamma energy decay (Table 6).

Table 6. Specific activity (Bq/kg)

ISGS code	Sample	238U	226Ra	210Pb	232Th	40K
798	MLm047b	11.6 ± 1.5	11.4 ± 0.2	10.8 ± 1.1	15.7 ± 0.3	305 ± 6
799	MLm065c	22.1 ± 1.5	16.1 ± 0.5	19.0 ± 1.8	17.7 ± 0.4	284 ± 8
800	AS05SEP21-1	14.8 ± 1.1	16.0 ± 0.2	16.7 ± 1.1	14.34 ± 0.26	365 ± 6
801	AS05SEP21-2	10.4 ± 1.2	12.1 ± 0.3	6.5 ± 1.4	10.50 ± 0.29	320 ± 8
802	AS05SEP21-4	16.9 ± 1.5	12.93 ± 0.32	14.5 ± 1.5	13.00 ± 0.31	324 ± 7
803	AS05SEP21-5	48.6 ± 2.0	41.6 ± 0.5	37.6 ± 1.6	33.2 ± 0.6	413 ± 7

For K-feldspar, we assumed an internal content of  $12.5 \pm 0.5$  % and  $400 \pm 100$  ppm, for potassium and rubidium, respectively (Huntley and Baril, 1997; Huntley and Hancock, 2001). A conservative  $0.10 \pm 0.05$  “a value” (efficiency of alpha particles compared with beta particles upon inducing a trapped charge in quartz and feldspar; i.e., alpha is only 10% as effective as beta) was retained (Table 7).

There is a slight deficit in radium 226, relative to its parent uranium 238, for samples ISGS 799, 802, and 803. Also, we observed a slight deficit in lead 210, relative to its parent radium 226, for samples 801 and 803. A deficit highlights a chemical mobility in the sediment, promoted by water: radium is easily dissolved (Ivanovich and Harmon, 1992). When 226Ra is lower than 238U, it means radium was leached, < recently > (not more than 5x the half-life of 226Ra, or 8000 years). When 210Pb is lower than 226Ra, it means that radium was precipitated in this sediment, < recently > (not more than 5x the half-life of 210Pb, or 100 years). Figure 5 (from Argonne National Laboratory) shows the uranium series radioactive decay, from uranium 238 all the way to lead 206 (stable). The ages shown are the half-lives, for each radioisotope. Fortunately, here, these sediments contain a lot of potassium, and comparatively less uranium. Potassium contributes for the vast majority of the dose rate, both externally (i.e. the sediment) and internally (the K, inside K-feldspar minerals). The dose rate contribution from radium 226 and lead 210, relative to the total dose rate, amounts to 9 %. Here, the uranium disequilibrium (deficit in radium 226, lead 210) affects a portion of this 9 %. It is very likely that this mobility was triggered < recently >, as the river migrates in its channel.

Table 7. Contribution to the dose rate, expressed in Gy/ka

ISGS code	alpha external (Gy/ka)	beta internal (Gy/ka)	beta external (Gy/ka)	gamma (Gy/ka)	cosmic ray (Gy/ka)	depth (m)	total (Gy/ka)
798	0.03 ± 0.02	0.87 ± 0.04	0.69 ± 0.04	0.41 ± 0.01	0.03 ± 0.01	24	2.04 ± 0.06
799	0.05 ± 0.03	0.81 ± 0.04	0.69 ± 0.05	0.43 ± 0.01	0.02 ± 0.01	43	2.00 ± 0.07
800	0.06 ± 0.04	0.57 ± 0.03	0.97 ± 0.07	0.53 ± 0.02	0.13 ± 0.01	4	2.26 ± 0.08
801	0.03 ± 0.02	0.81 ± 0.04	0.81 ± 0.06	0.44 ± 0.02	0.14 ± 0.01	4	2.23 ± 0.08
802	0.04 ± 0.03	0.81 ± 0.04	0.87 ± 0.07	0.47 ± 0.02	0.04 ± 0.01	20	2.23 ± 0.08
803	0.10 ± 0.06	0.81 ± 0.04	1.21 ± 0.07	0.85 ± 0.02	0.15 ± 0.01	4	3.12 ± 0.10

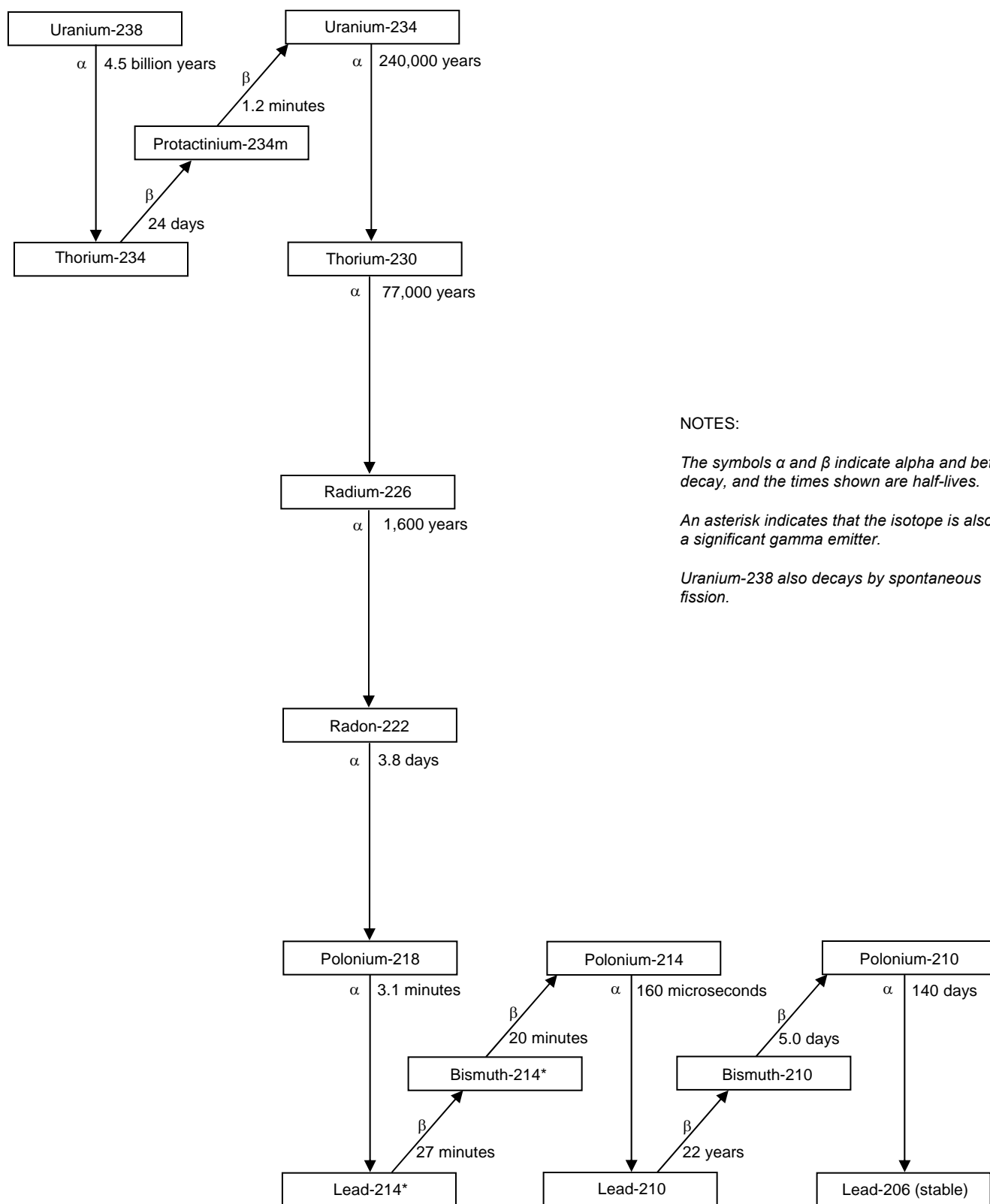


**Figure 5 Natural Decay Series: Uranium-238**

The beta dose rate absorption efficiencies were adjusted according to the specific grain size and mineral used for equivalent dose measurement (Nathan, 2010). External beta and gamma contributions were attenuated for water content (Zimmerman, 1971). The energy-to-dose rate conversion coefficient relied on the update by Guérin et al. (2011). Cosmic ray contributions were calculated from Prescott and Hutton (1988; 1994).

#### 4. Uncertainty budget

The breakdown of the uncertainties, between the total random and systematic sources, are presented in table 8. The random uncertainties reflect the standard error on the best estimate (i.e. from the central age model) for the equivalent dose (in seconds of laboratory-induced irradiation). The systematic uncertainties reflect here the combined (in quadrature) components of the environmental dose rate and calibration of the beta source on the luminescence system.

Table 8. Random and systematic uncertainties (in years), at 1 sigma

ISGS code	Sample	Age (ka)	1 $\sigma$ (random)	1 $\sigma$ (systematic)
798	MLm047b	187.040 $\pm$ 29.274	$\pm$ 28.574	$\pm$ 6.363
799	MLm065c	142.582 $\pm$ 19.068	$\pm$ 18.362	$\pm$ 5.141
800	AS05SEP21-1	42.291 $\pm$ 4.718	$\pm$ 4.412	$\pm$ 1.670
801	AS05SEP21-2	49.067 $\pm$ 5.440	$\pm$ 5.115	$\pm$ 1.854
802	AS05SEP21-4	40.004 $\pm$ 3.439	$\pm$ 3.050	$\pm$ 1.588
803	AS05SEP21-5	21.485 $\pm$ 1.574	$\pm$ 1.364	$\pm$ 0.785

#### 5. Conclusion

In summary, quartz minerals displayed undesirable luminescence characteristics. A reliable age could be not determined from them. Instead, the age was obtained with K-feldspar. These samples behaved reasonably well. The dose rate was derived from present-day values. Anomalous fading was measured and corrected with a single aliquot approach. Both MLm samples are old, but not THAT old!

Sebastien Huot, PhD

Illinois State Geological Survey

## References

- Aitken, M.J., 1998. An introduction to optical dating. Oxford University Press, Oxford.
- Auclair, M., Lamothe, M., Huot, S., 2003. Measurement of anomalous fading for feldspar IRSL using SAR. *Radiation Measurements* 37, 487-492.
- Brooks, C., Hart, S.R., Wendt, I., 1972. Realistic use of two-error regression treatments as applied to rubidium-strontium data. *Reviews of Geophysics* 10, 551-577.
- Buylaert, J.P., Murray, A.S., Huot, S., 2008. Optical dating of an Eemian site in Northern Russia using K-feldspar. *Radiation Measurements* 43, 715-720.
- Galbraith, R.F., Roberts, R.G., Laslett, G.M., Yoshida, H., Olley, J.M., 1999. Optical dating of single and multiple grains of quartz from Jinmium rock shelter, northern Australia: part I, experimental design and statistical models. *Archaeometry* 41, 339-364.
- Gilmore, G.R., 2008. Practical gamma-ray spectrometry, 2nd ed. John Wiley & Sons, Ltd.
- Godfrey-Smith, D.I., Huntley, D.J., Chen, W.H., 1988. Optical dating studies of quartz and feldspar sediment extracts. *Quaternary Science Reviews* 7, 373-380.
- Guérin, G., Mercier, N., Adamiec, G., 2011. Dose-rate conversion factors: update. *Ancient TL* 29, 5-8.
- Huntley, D.J., Baril, M.R., 1997. The K content of the K-feldspars being measured in optical dating or in thermoluminescence dating. *Ancient TL* 15, 11-13.
- Huntley, D.J., Hancock, R.G.V., 2001. The Rb contents of the K-feldspar grains being measured in optical dating. *Ancient TL* 19, 43-46.
- Huntley, D.J., Lamothe, M., 2001. Ubiquity of anomalous fading in K-feldspars and the measurement and correction for it in optical dating. *Canadian Journal of Earth Sciences* 38, 1093-1106.
- Huot, S., Lamothe, M., 2003. Variability of infrared stimulated luminescence properties from fractured feldspar grains. *Radiation Measurements* 37, 499-503.
- Ivanovich, M., Harmon, R.S., 1992. Uranium-series disequilibrium: Applications to Earth, Marine and Environmental Sciences. Clarendon Press, Oxford.
- Krbetschek, M.R., Götze, J., Dietrich, A., Trautmann, T., 1997. Spectral information from minerals relevant for luminescence dating. *Radiation Measurements* 27, 695-748.
- Ludwig, K.R., 2003. Mathematical-statistical treatment of data and errors for Th-230/U geochronology, in: Bourdon, B., Henderson, G.M., Lundstrom, C.C., Turner, S.P. (Eds.), *Uranium-Series Geochemistry*. Mineralogical Society of America, pp. 631-656.
- Murray, A.S., Wintle, A.G., 2000. Luminescence dating of quartz using an improved single-aliquot regenerative-dose protocol. *Radiation Measurements* 32, 57-73.
- Nathan, R.P., 2010. Numerical modelling of environmental dose rate and its application to trapped-charge dating. University of Oxford, Oxford, UK, p. 207.
- Prescott, J.R., Hutton, J.T., 1988. Cosmic ray and gamma ray dosimetry for TL and ESR. *Nuclear Tracks and Radiation Measurements* 14, 223-227.
- Prescott, J.R., Hutton, J.T., 1994. Cosmic ray contributions to dose rates for luminescence and ESR dating: Large depths and long-term time variations. *Radiation Measurements* 23, 497-500.
- Wintle, A.G., 1973. Anomalous fading of thermoluminescence in mineral samples. *Nature* 245, 143-144.
- Zimmerman, J., 1971. The radiation-induced increase of the 100°C thermoluminescence sensitivity of fired quartz. *Journal of Physics C: Solid State Physics* 4, 3265-3276.